Major classification: Biological Sciences

Minor classification: Microbiology

Herpesviral Replication Compartments Move and Coalesce at Nuclear Speckles to Enhance Export of Viral Late mRNA

Lynne Chang[1], William J. Godinez[2], Il-Han Kim[2], Marco Tektonidis[2], Primal de Lanerolle[3], Roland Eils[2], Karl Rohr[2], and David M. Knipe[1]

[1]Dept. of Microbiology and Molecular Genetics, Harvard Medical School, Boston, MA, 02115, USA

[2]Dept. of Bioinformatics and Functional Genomics, Biomedical Computer Vision Group, BIOQUANT, IPMB, University of Heidelberg and DKFZ Heidelberg, 69120 Heidelberg, Germany

[3]Dept. of Physiology and Biophysics, College of Medicine, University of Illinois at Chicago, Chicago, IL, 60612, USA

Corresponding author: David M. Knipe
Harvard Medical School
200 Longwood Avenue
Armenise Bldg. Rm 530
Boston, MA, 02115, USA
Ph) 617-432-1934
Fax) 617-432-0223
Email) david_knipe@hms.harvard.edu

Abstract

The role of the intranuclear movement of chromatin in gene expression is not well understood. Herpes simplex virus forms replication compartments (RCs) in infected cell nuclei as sites of viral DNA replication and late gene transcription. These structures develop from small compartments that grow in size, move and coalesce. Quantitative analysis of RC trajectories, derived from 4D images, show that most RCs move by directed motion. Directed movement is impaired in the presence of actin and myosin inhibitors as well as a transcription inhibitor. In addition, RCs coalesce at and reorganize nuclear speckles. Lastly, distinct effects of actin and myosin inhibitors on viral gene expression suggest that RC movement is not required for transcription but rather, movement results in the bridging of transcriptionally active RCs with nuclear speckles to form structures that enhance export of viral late mRNAs.

\body

Introduction

Movement of chromatin and its interactions and location in the nucleus are believed to be important for regulation of gene expression (1). A number of studies have shown an association between the movement of chromosomal domains and changes in transcriptional activity. In yeast, activation of genes is associated with targeting of the gene to the nuclear periphery (2, 3), and this is believed to be due to the linkage of actively transcribed genes to the nuclear pore complex for RNA export (4). Lymphoid cell genes move to positions near centromeric heterochromatin coincident with transcriptional silencing (5). Transcriptional activation of the β-globin locus involves movement of the gene away from centromeric heterochromatin (6). During B cell development the IgH and Igκ loci are localized at the nuclear periphery in hematopoietic progenitor cells, but they move internally coincident with transcriptional activation in pro-B cells (7). Similarly, the β-globin gene relocalizes to the nuclear interior as it is activated during murine erythroid differentiation (8). Actively transcribed genes are also thought to be brought into close contact with nuclear speckles (9, 10), sites often regarded as hubs of RNA metabolism. Although these results link gene movement with changes in transcriptional activity, it is unclear whether intranuclear movement of chromatin is the cause or the result of changes in transcriptional activity (1). Therefore, it is important to define systems in which the function of chromatin movement can be experimentally assessed.

Nuclear forms of actin and myosin have been implicated in mediating long-range, directed movement (11-13) but the mechanism by which this putative nucleoskeletal system operates is unknown. In addition to their possible roles in mediating intranuclear movement, there is increasing evidence for the roles of nuclear actin and myosin in cellular transcription, chromatin remodeling and mRNA export (reviewed in 14). How and whether their roles in movement are connected to regulation of gene activity is unclear.

Viruses are simple genetic entities and have often provided precise probes of cellular molecular mechanisms. Viral chromosomes of herpes simplex virus (HSV) are replicated and undergo late transcription in intranuclear structures called replication compartments (RCs; 15), which are known to move and coalesce in nuclei of infected cells during the course of infection (16, 17). The function and mechanism of RC movement are unknown. However, lepidopteran nucleopolyhedroviruses, large double-stranded DNA viruses that also replicate inside the host nucleus, have been shown to manipulate nuclear G- and F-actin for viral gene expression and progeny production (reviewed in 18). Pseudorabies virus and HSV have also been shown to induce F-actin formation in nuclei of certain cells and viral capsids appear to be associated with these structures (19, 20). Other studies have shown that HSV capsids undergo directed movement inside the nucleus (21), which is inhibited by the actin polymerization inhibitor latrunculin A (lat A) and the putative myosin inhibitor 2,3-butanedione monoxime (BDM; 22, 23). Based on the increasing evidence for the role of intranuclear movement in gene regulation and its involvement during viral

infection, we were interested in the possible roles for movement in HSV-1 gene expression.

HSV-1 transcription, DNA synthesis, and capsid assembly all occur in the nucleus and are temporally regulated by a cascade of immediate-early (IE), early (E), and late (L) gene expression. As mentioned above, these processes are also spatially regulated in the form of intranuclear compartmentalization (24). RCs, which were first identified by the presence of ICP8, an HSV single-stranded DNA binding protein (15), develop from small structures that grow in size, move and coalesce, ultimately filling the entire nucleus and marginalizing host chromatin to the nuclear periphery (17, 25-27). RCs have also been shown to be transcriptionally active by the presence of a viral transactivator protein ICP4 (28, 29) and RNA pol II (30) that co-localize with ICP8. To better understand the mechanism and function of intranuclear movement of RCs, we carried out 4D-imaging of cells infected with a recombinant HSV-1 strain expressing ICP8 fused to GFP to visualize RCs. Our results showed that the majority of RCs move by directed motion and require nuclear actin, myosin, and ongoing transcription. RC movement resulted in coalescence at nuclear speckles. Interestingly, inhibition of directed movement by lat A led to decreased accumulation of viral gene transcripts while inhibition by BDM resulted in a defect in export of a late viral mRNA. Combined, our data suggest that HSV RC movement results in bridging transcriptional domains within RCs to RNA processing structures in the nucleus to enhance export of a subset of late viral mRNAs.

Results

RCs move by an active process

To better understand the process of RC movement in the context of the 3-dimensional nucleus, we carried out 4-dimensional (3-D space and time) confocal imaging of cells infected with a recombinant HSV-1 strain expressing ICP8 fused to GFP (8GFP virus; 17). Cells were imaged from 4 to 7 hours post infection (hpi). ICP8-GFP localized to bright foci clustered within RCs. Smaller and dimmer individual foci, most likely representing viral pre-replicative sites (15), were also present along the nuclear periphery and in the nucleoplasmic space between RCs (Figure 1). These smaller individual foci exhibited highly constrained movement while whole RCs displayed long-range movement, often toward another RC (Figure 1 and Movie S1). When the movement of RCs was tracked relative to the position of the nucleus in the 4D datasets, these structures moved at an average speed of 0.24 μm/min (up to 0.35 μm/min; SD = 0.056 μm/min). RCs traveled distances of up to 5.65 μm during the 3-hour imaging period (as calculated by the shortest distance between the first and last frame for the longest track). The observed distances traveled by RCs and the average speed of movement are comparable to published reports of long-distance movement of chromosomal loci (11).

To quantify RC movement more rigorously, we developed a motion classification approach based on both the anomalous diffusion coefficient (α; 31) and 3D relative shape anisotropy (κ^2; 32, 33; see Supporting Information for definitions). To obtain an estimate for α, of each trajectory, we computed the

mean-square displacement (MSD) as a function of the time interval, Δt. To improve the accuracy of the estimates (31), we restricted the MSD calculations to Δt values less than $N/3$, where N is the total number of available positions in the trajectory. The motion properties of immobile RCs and those exhibiting either constrained or diffusive motion were already manifest over short time intervals, so the computed α value correlated well with these types of motion. However, because the motion properties of RCs displaying directed motion were evident only at a larger temporal scale, the computed value for α often did not characterize this type of motion accurately. Because the positions representing a directed motion trajectory exhibit a highly anisotropic scatter, a more effective way to detect this type of motion was to characterize the shape of the trajectory via its 3D relative shape anisotropy κ^2 (32; see Figure 2A for sample RC trajectories, their ellipsoid of gyration, and κ^2 values, which are defined as a function of the squared lengths of the semi-axes of the ellipsoid). Our hierarchical approach for determining the motion type of the RCs therefore first employed κ^2 to distinguish trajectories exhibiting directed motion from those displaying random motion. Trajectories with isotropic shapes were then further classified into confined diffusion, obstructed diffusion, or simple diffusion, based on their α values and the classification scheme in Bacher et al. (34; see Figure 2B for sample MSD curves that correspond to trajectories shown in Figure 2A). Based on this hierarchical analysis approach, 74% of RCs appeared to undergo directed motion, 13% displayed simple diffusion and 13% displayed obstructed diffusion (Figure 2C; control; n=5 nuclei, 23 RCs analyzed). None of the RCs

displayed confined diffusion. These results showed that the majority of the RCs moved by an active process.

Active movement of RCs depends on nuclear actin, myosin I and transcription

Active movement of transgenes has been reported to involve nuclear actin and nuclear myosins such as nuclear myosin I (NMI; 11-13). To determine if nuclear myosin was involved in the active transport of RCs, we treated cells with BDM at 3 hpi and imaged the cells from 4-7 hpi. Because BDM also affects cytoplasmic myosin function, we treated cells with BDM starting at 3 hpi to allow unobstructed viral entry and to minimize potential effects on cytoplasmic trafficking of incoming virions, which could in turn affect RC growth and dynamics. An average of four nuclei and 22 RCs were analyzed per treatment to determine the distribution of motion types as described in the previous section. BDM-treated cells showed a significant decrease in the fraction of RCs undergoing directed motion and an increase in RCs undergoing obstructed diffusion (Figure 2C; p=0.011, Table S1). To determine the role of nuclear actin in RC movement, we also treated cells with lat A at 3 hpi. Treatment with this drug also led to a significant decrease in the fraction of RCs undergoing directed motion and an increase in those undergoing obstructed diffusion (Figure 2C; p=0.006, Table S1). It should be noted that viral entry and cytoplasmic trafficking of HSV-1 in Vero cells, the cell type used in our experiments, occur

independently of actin (35), consistent with the effects of lat A affecting nuclear and not cytoplasmic viral functions.

To determine whether nuclear myosin I (NMI) was specifically involved in the directed movement, we transfected cells with a plasmid expressing a dominant-negative form of NMI (NMI-E407V). NMI-E407V is a mutant form of NMI that has impaired actin binding and motor activity and has been shown to reduce chromosomal loci movement (11). Expression of NMI-E407V led to a decreased number of RCs undergoing directed motion (Figure 2C; p=0.001, Table S1). To confirm the effects of lat A, we also transfected cells with a construct encoding a dominant-negative form of nuclear actin (actin-G13R). Actin-G13R contains an NLS sequence and is a non-polymerizable mutant form of actin, which has been shown to inhibit long-range movement of chromosomal loci (11). Expression of actin-G13R also led to a decrease in the fraction of RCs undergoing directed motion (Figure 2C; p=0.013, Table S1). However, the effect was not due entirely to the dominant negative mutation because cells transfected with a plasmid encoding a YFP-tagged, nuclear-targeted wild-type actin (actin-NLS) also showed a decrease in the fraction of RCs undergoing directed motion (Figure 2C; p=0.038, Table S1). All cells (including controls) were co-transfected with a plasmid encoding mCherry-tagged lamin A (mCh-LA) to correct for nuclear rotation and translation during RC tracking analysis. Therefore, the observed inhibitory effect is most likely not due to non-specific effects of over-expressing a nuclear protein.

Previous studies had shown that transcription is involved in long-range movement of chromosomal loci (12, 36). Therefore, we treated cells with the RNA pol II inhibitor, α-amanitin, at 4 hpi. The α-amanitin treatment led to a significant decrease in directed movement (Figure 2C; p=0.002, Table S1). In contrast, treatment of cells with a protein synthesis inhibitor, cycloheximide, at 4 hpi did not lead to a significant change in the distribution of movements (Figure 2C; p=0.355, Table S1). These results argued that directed RC movement involves nuclear actin, myosin and ongoing transcription.

RCs coalesce at nuclear speckles

Previous studies have reported the clustering of co-regulated genes at nuclear speckle bodies (9, 13, 37). To determine whether RCs were coalescing at speckles, we first carried out indirect immunofluorescence analysis of infected cells at various times post infection using antibodies specific for SC35, one of the major components of speckles, and for ICP8. In the resulting time-series of images (Figure 3A), RCs were frequently found adjacent to SC35-positive speckles. In some cases, speckles were associated with more than one RC, and some RCs were associated with more than one speckle (see 5hpi panel). Both RCs and speckles were re-organized so that by 6hpi, many cells contained large RCs bordered by a few large speckles (see 6hpi panel in Figure 3A). To determine if movement or transcription played a role in this association, we treated cells with either lat A, BDM or control medium at 1hpi or with α-amanitin at 4 hpi. When fixed and processed at 4.5hpi, all cells showed RCs associated

with speckles, including those treated with the various drugs (Figure 3B). Speckle bodies appeared rounder and smaller in α-amanitin-treated cells, and lat A-treated cells exhibited nuclei that were smaller and more convoluted but the majority of RCs were still found adjacent to speckle bodies. These results argued that the initial association between RCs and speckles did not depend on actin or myosin.

To examine potential interactions between speckles and RCs in live cells, we transfected cells with a plasmid encoding mCherry-tagged SC35 protein (mCh-SC35). At 24 hrs post transfection, we infected the cells with 8GFP virus and started imaging them at 4 hpi (Figure 4A and Movie S2). mCh-SC35 localized to structures that resembled speckle bodies. At 4 hpi, the majority (78%) of RCs were adjacent to these SC35-positive speckles. Live-cell imaging revealed that ~91% of RCs coalesced, and 100% of these coalescence events occurred in association with a speckle body. Three main types of RC movement patterns relative to speckles were observed: independent movement of RCs (type 1) that either resulted in contact with a speckle (Figure 4A-1a) or with an RC that was associated with a speckle (Figure 4A-1b); movement of RC on the surface of a speckle (type 2; Figure 4B-2); and movement of RCs with speckles (type 3; Figure 4B-3). Speckles were also observed to merge during type 3 movement. Approximately 42% of RCs moved independently, ~40% moved on the surface of a speckle, and ~7% moved with a speckle (Figure 4C). The number of RCs moving on the surface of a speckle may be under-estimated because such movement was only identifiable when there were at least two RCs

on a common speckle where one could serve as a fiducial mark. To determine which of these three types of movement required actin, myosin or transcription, we treated cells with control, lat A, or BDM medium at 3 hpi or with α-amanitin at 4 hpi (Movies S3-5). An average of 7 nuclei and 44 RCs were analyzed per treatment. Lat A, BDM and α-amanitin treatment all led to significant reductions in the number of coalescence events (Figure 4C). In addition, all three treatments also led to significant reductions in both types 1 and 2 movements (Figure 4C), indicating that actin, myosin and transcription could be involved in mediating these movements. These drugs did not have a significant effect on type 3 movement. However, the frequency of this type of movement was also low in control cells compared to types 1 and 2.

Effects of directed RC movement on viral gene expression and DNA replication

To determine the possible role(s) for directed movement of RCs in viral gene expression, we infected cells with HSV-1 and treated them with either lat A, BDM or control medium at 3 hpi. We harvested cells at 3, 7, and 12 hpi, and measured RNA and protein levels of three genes, *ICP27*, *ICP8* and *gC*, representative of the IE, E, and L HSV genes, respectively. RNA levels were measured by reverse-transcription and quantitative real-time PCR (RT-qPCR), and protein levels were determined by SDS-PAGE and Western blot analysis. At 12 hpi, lat A-treated cells contained reduced levels of all three transcripts compared to control medium-treated cells (Figure 5A). Furthermore, there was a

corresponding decrease in levels of the three proteins with the largest decrease in gC level at 12 hpi (71% decrease; Figure 5B,C). In contrast, BDM treatment resulted in increased accumulation of both *ICP27* and *ICP8* mRNAs by 12 hpi as compared to control medium (Figure 5A). *gC* mRNA levels in BDM-treated cells were similar to control medium-treated cells (Figure 5A). However, the effects of BDM on protein levels were similar to lat A-treated cells with modest reductions in ICP27 and ICP8 and a significant reduction in gC level (79% reduction; Figure 5B,C). Therefore, lat A treatment reduced viral RNA levels generally while BDM treatment specifically inhibited the protein levels of *gC*.

To determine if inhibition of directed RC movement affected viral DNA replication, we harvested cells treated with lat A, BDM or control medium at 3, 7 and 12 hpi for DNA isolation. DNA samples were analyzed by real-time PCR, using primers specific for the *ICP27* gene, to determine viral DNA levels. At 7 hpi, lat A- and BDM-treated cells contained ~59% and ~69% of viral DNA found in control cells, respectively (Figure 5D). At 12 hpi, lat A-treated cells contained ~68% of viral DNA found in control cells and BDM-treated cells contained ~67% (Figure 5D). The reduced level of viral DNA in these cells may be a result of the observed decreased levels of IE and E proteins that regulate viral DNA replication or by direct inhibition of replication by the drugs.

Effects of directed RC movement on nuclear export of *gC* mRNA

The contrasting effects of BDM on *gC* mRNA and protein levels led us to examine whether inhibition of RC movement by BDM had an effect on nuclear

export of *gC* mRNA. We incubated cells with lat A, BDM or control medium at 3 hpi, as described above, harvested the cells at 12 hpi for isolation of nuclear and cytoplasmic RNA, and determined the amounts of RNA by Northern blotting, or by RT-qPCR to determine relative amounts of *gC* transcripts (Figure 6A). Lat A treatment did not significantly affect the nuclear-cytoplasmic distribution of *gC* transcripts. In contrast, BDM treatment led to a ~2 fold increase in the percent of *gC* mRNA present in the nucleus, as compared to cells treated with control medium. BDM treatment did not affect the percentage of *ICP27* and *ICP8* transcripts in the nucleus (Figure 6B). The percentage of *ICP5* mRNA encoded by a leaky-late gene, in the nucleus, was also not affected by BDM (Figure 6B). These results suggested a role for myosin-mediated RC movement in the nuclear export of a subset of viral late mRNAs, perhaps true late gene transcripts, such as gC.

Discussion

Movement of RCs

Our results show that approximately three fourths of HSV RCs move in infected cell nuclei by directed motion. The distance (up to 5.65 μm) and average speed of RC movement (0.24 μm/min) are comparable to values reported for long-range movement of chromosomal loci (11). RC movement requires nuclear actin, myosin and ongoing transcription. Furthermore, movement results in coalescence of RCs at speckles and re-organization of speckle bodies. Because speckles are considered to be hubs of transcription,

RNA splicing, processing and export (reviewed in 37, 38), the observed interactions between RCs and speckles further support the idea that RC movement is related to RNA metabolism events.

Association with nuclear speckles

HSV infection has long been known to reorganize speckles into larger bodies (39) with ICP27 being required for this reorganization (40, 41). Reorganization of speckles may be the result of 1) inhibition of host RNA splicing events, which in turn contributes to the inhibition of cellular gene expression (reviewed in 42); 2) an indirect effect of inhibiting cellular transcription; or 3) an active process at least in part due to the RC and speckle movement shown here. Unlike cellular pol II transcripts, the majority of HSV transcripts are intronless. Because splicing and RNA processing events are closely linked to nuclear export, in the absence of splicing, RCs may need to reorganize and associate with speckle bodies to recruit RNA processing and nuclear export factors to sites of true late viral gene transcription on progeny viral DNA molecules.

Similar reorganization of nuclear speckles is known to occur in response to heat shock (reviewed in 43) and inhibition of transcription by α-amanitin (44, 45). Recent studies showed that heat-shock induced *Hsp70* transgenes associated with nuclear speckles in a dynamic fashion (46), and this association was promoter- and transcription-dependent (47). Despite the dependence on transcription, the level of accumulated nascent transcript did not appear to be critical for speckle association. Other studies involving the association of heat

shock genes with speckles showed that this association was independent of the presence of introns (48). However the functional significance of the association remains unclear. Other studies have shown that in cells where transcription was inhibited by α-amanitin or heat shock, RNA pol II and splicing factors accumulated in speckles (45). The authors speculate that these results reflect the role of speckles as recycling centers for transcription and splicing factors especially during periods of transcription inactivation. Therefore, association of HSV-1 RCs with nuclear speckles may be a method to take advantage of the heightened concentration of these factors in speckles during infection when host transcription is shut down.

We found that the initial association of RCs with speckles did not require actin- and myosin-mediated movement because treatment of cells with lat A or BDM at 1hpi did not inhibit association between individual RCs and speckle bodies by 4.5hpi. This initial association could be formed either by diffusion or de-novo formation of speckles adjacent to RCs. Such de novo formation of speckle bodies has been reported for cellular transgenes (46). Promyelocytic leukaemia nuclear bodies (PML) have also been shown to form de novo and in association with viral genomes at early times post infection (49). This association is part of an intrinsic cellular defense mechanim that represses viral transcription and is counteracted by the viral regulatory protein ICP0, which induces subsequent degradation of PML (50). It will be interesting to determine if these early ND10-associated viral genomes are also associated with speckle bodies and if so, what the spatial and temporal relationships among these three

structures are. In contrast to the initial actin- and myosin-independent association, coalescence of RCs at speckles requires actin- and myosin-mediated movement. These results suggest that it is not the mere association with speckles but rather movement of RCs post-association with speckles and the act of coalescence on the surface of speckles that enhance *gC* mRNA export. Recent studies showed the presence of myosin Va (51) and proteins that regulate actin polymer dynamics such as PIP2, profilin and protein 4.1 in nuclear speckles (reviewed in 52). These observations present interesting possibilities regarding the recruitment of myosin and F-actin regulators from speckles to initiate RC movement.

Role for directed RC movement in viral late mRNA export

Surprisingly, lat A and BDM treatment, both of which inhibited movement, resulted in differing effects on viral gene expression with lat A leading to a general reduction in the accumulation of viral transcripts and BDM leading to a defect in the nuclear export of *gC* mRNA. BDM's effect on nuclear export may be specific for true late transcripts, as export of the leaky late ICP5 mRNA was not affected. This result argues that the inhibition of *gC* mRNA export is most likely a result of inhibiting RC movement and not a result of general export inhibition by BDM at late times post infection. BDM treatment may also inhibit other post-transcriptional processing events because the ~2 fold increase in nuclear accumulation of *gC* transcript may not be sufficient to explain the ~79% reduction in gC protein levels at 12 hpi. Alternatively, because degradation of

unprocessed mRNA precursors is known to occur in the nucleus (53), our results could be an underestimation of the defect in export. Interestingly, lat A treatment appeared to lead to decreased accumulation of nuclear *ICP5* mRNA. This result raises the possibility that not all viral genes share a requirement for actin and/or myosin.

We hypothesize that the differing effects on gene expression of two drugs that both inhibit movement of RCs could be that the inhibition of movement by one is indirect and the other is direct. Actin has been shown previously to be part of pre-initiation complexes and required for transcription by RNA pol II (54). In our model, lat A treatment which inhibited transcription, could inhibit movement indirectly. In contrast, BDM treatment, which inhibited nuclear export, may inhibit movement directly. We speculate that myosin is recruited specifically to RCs involved in transcription of true late genes, triggering directed movement towards hubs of RNA processing and export (Figure 7). It is surprising that BDM treatment did not lead to decreased levels of mRNA because NMI has been shown previously to stimulate basal transcription by RNA pol II (55). This may indicate differences between cellular and viral gene transcription or that BDM treatment may affect a different or broader range of myosin isoforms. Alternatively, BDM has also been shown to affect the recruitment of proteins involved in actin polymerization such as the Arp 2/3 complex (23). It is possible that the inhibition of RC movement by BDM is related to its effects on actin polymer dynamics that is distinct from lat A-mediated effects on actin and that this property in turn, is involved in post-transcriptional events.

Regardless of the mechanism behind the effects of lat A and BDM on RC movement, the inhibition of movement by α-amanitin treatment combined with the differing effects on viral gene expression by lat A and BDM treatments argue that movement is not required for transcription but rather that transcription is required for movement (Figure 7). Our results are consistent with previous studies demonstrating the involvement of transcription in mediating movement of genetic loci (12, 47, 36, reviewed in 1). Furthermore, our results showing that BDM treatment inhibits movement without reducing transcript levels, raises the possibility that transcription alone does not induce movement but rather the recruitment of post-transcriptional processing factors (that are dependent on transcription) may be the trigger for movement. Determination of the exact mechanisms by which actin, myosin, transcription and RNA processing events cause movement will require further studies.

Finally, our live cell imaging experiments show that the majority of RC movement results in fusion of two or more RCs at speckle bodies. We hypothesize that the fusion of RCs could lead to a structural reorganization in both compartments allowing for more efficient incorporation of RNA processing factors and/or for the translocation of RNAs into the associated speckle body for processing, thus leading to the formation of a hub that is optimized for processing and export of a subset of late mRNAs (Figure 7). It will be important to determine if RC movement affects export of other viral transcripts and if so, to determine whether they share similar RNA export or processing requirements.

The highly dynamic HSV RCs provide a useful tool for investigating the mechanism and function of intranuclear movement and interchromosomal interactions in living cells. Our results support the idea that the dynamic nature and positioning of genetic material within the complex nuclear architecture plays an essential role in the expression of eukaryotic genes. The movement of actively transcribed genes to sites of RNA processing and export may be a general mechanism that eukaryotic cells and viruses use to optimize the efficiency of coupling of transcription to RNA processing and nuclear export.

Experimental Procedures

Cells and viruses

Vero cells used for RNA, protein and DNA isolation, and immunofluorescence analysis were grown and maintained in DMEM+10%S (Dulbecco's modified Eagle's medium (DMEM) with 5% fetal bovine serum (FBS), 5% bovine calf serum (BCS), glutamine). For live-cell imaging studies, an ICP8-complementing cell line, V529 (56), was used. V529 cells were grown and maintained in DMEM+10%S containing 400 μg/ml of G418. The ICP8-GFP recombinant virus (8GFP) used for live cell imaging experiments is described in Taylor et al. (17). 8GFP virus was propagated on V529 cells. The HSV-1 wild-type strain KOS used in the rest of the experiments was propagated on Vero cells.

Infection

For live-cell imaging experiments, V529 cells were infected with the 8GFP virus at multiplicity of infection of 10. Vero cells were infected with KOS at a moi of 10. At 1hr post incubation with either virus, unabsorbed virus was inactivated by treatment with acid wash (40 mM citric acid, 135 mM NaCl, 10 mM KCl, pH 3.0). Acid wash was then replaced with DMEV (DMEM with 1% BCS, glutamine, streptomycin and penicillin). For live-cell imaging, DMEV was replaced with phenol-free L-15, 1% BCS and glutamine at 4 hpi for the duration of the imaging period.

Transfections

Cells were transfected with plasmids using the QIAGEN Effectene transfection reagent 24 hrs prior to infection. For tracking experiments, cells were transfected with either mCh-LA alone (for drug treatments) or doubly transfected with mCh-LA and an actin/myosin plasmid (for dominant-negative experiments). Details regarding the plasmids used can be found in the Extended Experimental Procedures.

Drugs

Cells were treated with DMEV containing 0.03% DMSO (control medium), 1mM latrunculin A (lat A; Invitrogen), 20mM 2,3-Butanedione monoxime (BDM; Sigma-Aldrich), 10mM α-amanitin (Sigma-Aldrich), or 100 μg/ml cycloheximide (Sigma-Aldrich). For live-cell imaging experiments, drugs were included in the imaging medium.

Microscopy

The imaging system consisted of a fully motorized, inverted microscope (Zeiss Axiovert 200M) with a piezo-driven stage (Applied Scientific Instrument), enclosed in an environmental chamber, coupled to a computer controlled spherical aberration correction device (Intelligent Imaging Innovations.), a Yokogawa spinning disk confocal head (Perkin Elmer), and a back-illuminated EM-CCD camera (Cascade, Roper Scientific, Photometrics). 50mW solid-state lasers (488nm and 568nm, Crystal Laser, Reno, NV), controlled by an acousto-optical tunable filter were used for illumination. The image acquisition software used was SlideBook 4.2 (Intelligent Imaging Innovations). A Plan Apochromat 63x 1.4 N.A. lens (Carl Zeiss) was used. For 4D imaging, 3D stacks consisting of ~30 optical z-slices, 0.36μm apart were captured every 30sec-1min, for periods of up to 3 hrs.

4D tracking and motion analysis

Methods used for RC tracking and motion analyses are described in the Extended Experimental Procedures.

Indirect immunofluorescence

Wild-type HSV-1-infected Vero cells were fixed with 3.65% formaldehyde, permeabilized with 0.1% Triton-X 100, and incubated with antibodies for 30 mins at 37°C. Stained cells were mounted in ProLong Gold anti-fade reagent

(Invitrogen). A list of antibodies that were used and their dilutions can be found in the Extended Experimental Procedures.

RC-speckle dynamics analysis

To determine the distribution of the three types of movement in control versus drug treated cells, ~7 nuclei (~44 RCs) were analyzed per treatment. The three types of movement were defined qualitatively and the number of events counted manually. The number of RCs undergoing each type of movement was divided by the total number of RCs in each cell and presented as a percentage value. Student's t-test was used to determine the statistical significance of the differences between control and drug treated samples.

Western blots

Cells were lysed in SDS-PAGE loading buffer, and proteins were resolved by SDS-PAGE. Western blots were developed using Pierce ECL Western blotting substrate (Thermo Fisher Scientific). ImageJ software (http://rsb.info.nih.gov/ij/) was used to quantify the band intensities. Serial dilutions of the control 12 hpi protein sample were analyzed for each blot and each antibody to ensure linearity. Values were normalized to GAPDH and then to 12hpi values for each drug treatment. Experiments were conducted three times and their values averaged. A list of antibodies and the dilutions used can be found in the Extended Experimental Procedures.

Viral RNA RNA analysis by qPCR

Total RNA was extracted using the TRI-Reagent solution (Ambion) and DNase-treated using the DNA-*free* kit (Ambion). DNase-treated RNA (80 ng/sample) was then reverse-transcribed and quantified by real-time PCR (qPCR) as described in Cliffe et al. (57). Mock reverse-transcribed samples were included as negative controls. For nuclear-cytoplasmic fractionation, cells were lysed and fractionated according to the Supplemental protocol accompanying the QIAGEN RNeasy kit. RNA was extracted using the QIAGEN RNeasy mini kit, DNase treated as above, and quantified using the *Power* SYBR Green RNA-to-CT 1-step kit and a Prism 7300 sequence detection system (Applied Biosystems). All reactions were carried out in duplicate, and relative copy numbers determined by comparison with standard curves. Viral RNA levels were normalized to 18S rRNA levels and further normalized to control 12hpi values. Experiments were conducted three times, and the values were averaged. The Student's t-test was used to determine the statistical significance of differences between non-normalized control and drug-treated samples. Primer sequences can be found in the Extended Experimental Procedures.

Viral DNA analysis by qPCR

We used the QIAGEN DNeasy Blood and Tissue kit for DNA isolation. DNA amounts were analyzed using the *Power* SYBR Green PCR master mix and a Prism 7300 sequence detection system (Applied Biosystems). qPCR reactions were carried out in duplicate, and relative copy numbers were determined by

comparison with standard curves. Viral DNA levels were normalized to cellular sonic hedgehog gene (*SHH*) levels and then to control 12hpi values. Experiments were conducted three times and the values were averaged. Primer sequences can be found in the Extended Experimental Procedures.

Northern blot hybridization and analysis

The gC gene hybridization probe was prepared by cleavage of the pCI-gC plasmid (58). [^{32}P]dCTP labeling was carried out as described in Fontaine-Rogriguez et al. (59). Fractionated cytoplasmic and nuclear RNA samples from infected cells (described above) were resolved with a 1.5% agarose gel prepared with NorthernMax-Glyc gel prep/running buffer (Ambion). Resolved samples were transferred to a nylon membrane using Ambion's NorthernMax transfer buffer. Incubation with the probe was carried out in 5xSSPE (Boston BioProducts), 5xDenhardt's solution (Boston BioProducts), 50% formamide (Sigma-Aldrich), 0.5% SDS and 0.1 mg/ml of ssDNA (Invitrogen), for 48 hrs at 42°C. Membranes were exposed to film for autoradiography.

Acknowledgements

We thank Drs. Robert D. Goldman and Takeshi Shimi at Northwestern University Medical School for providing the mCh-lamin A construct, and Drs. Prasanth V. Kannanganattu at University of Illinois at Urbana-Champaign and David L. Spector at Cold Spring Harbor Laboratory for providing the mRFP-SC35 plasmid. We also thank the New England Regional Center for Excellence for Biodefense

and Emerging Infectious Diseases (National Institutes of Health Grant AI057159) imaging facility at the Immune Disease Institute for use of the spinning disk confocal microscope. Funding for this work was provided by NIH grant AI63106 to DMK and RO1GM080587 to PdL. Support for the project VIROQUANT (0313923) by the German Federal Ministry of Education and Research (BMBF) (FORSYS) is also acknowledged.

References

1. Hübner MR & Spector DL (2010) Chromatin dynamics. *Annu Rev Biophys* 99:471-489.
2. Brickner JH & Walter P (2004) Gene recruitment of the activated INO1 locus to the nuclear membrane. *PLoS Biol* 2: e342.
3. Casolari JM*, et al.* (2004) Genome-wide localization of the nuclear transport machinery couples transcriptional status and nuclear organization. *Cell* 117:427-439.
4. Blobel G (1985) Gene gating: a hypothesis. *Proc Natl Acad Sci U S A* 82:8527-8529.
5. Brown KE, Baxter J, Graf D, Merkenschlager M, & Fisher AG (1999) Dynamic repositioning of genes in the nucleus of lymphocytes preparing for cell division. *Mol Cell* 3:207-217.
6. Schübeler D*, et al.* (2000) Nuclear localization and histone acetylation: a pathway for chromatin opening and transcriptional activation of the human beta-globin locus. *Genes Dev* 14:940-950.
7. Kosak ST*, et al.* (2002) Subnuclear compartmentalization of immunoglobulin loci during lymphocyte development. *Science* 296:158-162.
8. Ragoczy T, Bender MA, Telling A, Byron R, & Groudine M (2006) The locus control region is required for association of the murine beta-globin locus with engaged transcription factories during erythroid maturation. *Genes Dev* 20:1447-1457.
9. Brown JM*, et al.* (2008) Association between active genes occurs at nuclear speckles and is modulated by chromatin environment. J Cell Biol 182:1083–1097.
10. Spector DL & Lamond AI (2010) Nuclear Speckles. *Cold Spring Harb Perspect Biol* 3:a000646.
11. Chuang CH*, et al.* (2006) Long-range directional movement of an interphase chromosome site. *Curr Biol* 16:825-831.
12. Dundr M*, et al.* (2007) Actin-dependent intranuclear repositioning of an active gene locus in vivo. *J Cell Biol* 179:1095-1103.

13. Hu Q*, et al.* (2008) Enhancing nuclear receptor-induced transcription requires nuclear motor and LSD1-dependent gene networking in interchromatin granules. *Proc Natl Acad Sci U S A* 105:19199-19204.
14. Visa N & Percipalle P (2010) Nuclear functions of actin. *Cold Spring Harb Perspect Biol* 2:a000620.
15. Quinlan MP, Chen LB, & Knipe DM (1984) The intranuclear location of a herpes simplex virus DNA-binding protein is determined by the status of viral DNA replication. *Cell* 36:857-868.
16. Sourvinos G & Everett RD (2002) Visualization of parental HSV-1 genomes and replication compartments in association with ND10 in live infected cells. *EMBO J* 21:4989-4997.
17. Taylor TJ, McNamee EE, Day C, & Knipe DM (2003) Herpes simplex virus replication compartments can form by coalescence of smaller compartments. *Virology* 309:232-247.
18. Volkman LE (2007) Baculovirus infectivity and the actin cytoskeleton. *Curr Drug Targets* 8:1075-1083.
19. Feierbach B, Piccinotti S, Bisher M, Denk W, & Enquist LW (2006) Alpha-Herpesvirus Infection Induces the Formation of Nuclear Actin Filaments. *PLoS Pathog* 2:e85.
20. Ecob-Johnston MS & Whetsell WO, Jr. (1979) Host-cell response to herpes virus infection in central and peripheral nervous tissue in vitro. *J Gen Virol* 44:747-757.
21. Forest T, Barnard S, & Baines JD (2005) Active intranuclear movement of herpesvirus capsids. *Nat Cell Biol* 7:429-431.
22. Ostap EM (2002) 2,3-Butanedione monoxime (BDM) as a myosin inhibitor. *J Muscle Res Cell Motil* 23:305-308.
23. Yarrow JC, Lechler T, Li R, & Mitchison TJ (2003) Rapid de-localization of actin leading edge components with BDM treatment. *BMC Cell Biol* 4:5.
24. Roizman B, Knipe DM, & Whitley RJ (2007) Herpes Simplex Viruses. *Fields Virology*, eds Knipe DM & Howley PM (Lippincott, Williams and Wilkins, Philadelphia), 5th Ed, pp 2501-2602.
25. de Bruyn Kops A & Knipe DM (1988) Formation of DNA replication structures in herpes virus-infected cells requires a viral DNA binding protein. *Cell* 55:857-868.
26. Simpson-Holley M, Baines J, Roller R, & Knipe DM (2004) Herpes simplex virus 1 U(L)31 and U(L)34 gene products promote the late maturation of viral replication compartments to the nuclear periphery. *J Virol* 78:5591-5600.
27. Monier K, Armas JC, Etteldorf S, Ghazal P, & Sullivan KF (2000) Annexation of the interchromosomal space during viral infection. *Nat Cell Biol* 2(9):661-665.
28. Knipe DM, Senechek D, Rice SA, & Smith JL (1987) Stages in the nuclear association of the herpes simplex virus transcriptional activator protein ICP4. *J Virol* 61(2):276-284.

29. de Bruyn Kops A, Uprichard SL, Chen M, & Knipe DM (1998) Comparison of the intranuclear distributions of herpes simplex virus proteins involved in various viral functions. *Virology* 252(1):162-178.
30. Rice SA, Long MC, Lam V, & Spencer CA (1994) RNA polymerase II is aberrantly phosphorylated and localized to viral replication compartments following herpes simplex virus infection. *J Virol* 68(2):988-1001.
31. Saxton MJ & Jacobson K (1997) Single-particle tracking: applications to membrane dynamics. *Annu Rev Biophys Biomol Struct* 26:373-399.
32. Theodorou DN & Suter UW (1985) Shape of unpreturbed linear polymers: Polypropylene. *Macromolecules* 18:1206-1214.
33. Saxton MJ (1993) Lateral diffusion in an archipelago. *Biophys. J* 64:1766-1780.
34. Bacher CP, Reichenzeller M, Athale C, Herrmann H, & Eils R (2004) 4-D single particle tracking of synthetic and proteinaceous microspheres reveals preferential movement of nuclear particles along chromatin - poor tracks. *BMC Cell Biol* 5:45.
35. Sodeik B, Ebersold MW, & Helenius A (1997) Microtubule-mediated transport of incoming herpes simplex virus 1 capsids to the nucleus. *Journal of Cell Biology* 136:1007-1021.
36. Tumbar T & Belmont AS (2001) Interphase movements of a DNA chromosome region modulated by VP16 transcriptional activator. *Nature Cell Biology* 3:134-139.
37. Hall LL, Smith KP, Byron M, & Lawrence JB (2006) Molecular anatomy of a speckle. *Anat Rec A Discov Mol Cell Evol Biol* 288:664-675.
38. Zhong XY, Wang P, Han J, Rosenfeld MG, & Fu XD (2009) SR proteins in vertical integration of gene expression from transcription to RNA processing to translation. *Mol Cell* 35:1-10.
39. Martin TE, Barghusen SC, Leser GP, & Spear PG (1987) Redistribution of nuclear ribonucleoprotein antigens during herpes simplex virus infection. *Journal of Cell Biology* 105:2069-2082.
40. Phelan A, Carmo-Fonseca M, McLaughlan J, Lamond AI, & Clements JB (1993) A herpes simplex virus type 1 immediate-early gene product, IE63, regulates small nuclear ribonucleoprotein distribution. *Proc Natl Acad Sci USA* 90:9056-9060.
41. Sandri-Goldin RM, Hibbard MK, & Hardwicke MA (1995) The c-terminal repressor region of herpes simplex virus type 1 ICP27 is required for the redistribution of small nuclear ribonucleoprotein particles and splicing factor SC35; however, these alterations are not sufficient to inhibit host cell splicing. *J Virol* 69:6063-6076.
42. Sandri-Goldin RM (2008) The many roles of the regulatory protein ICP27 during herpes simplex virus infection. *Front Biosci* 13:5241-5256.
43. Lamond AI & Spector DL (2003) Nuclear speckles: A model for nuclear organelles. *Nat Rev Mol Cell Biol* 4:605-612.
44. Carmo-Fonseca M, Pepperkok R, Carvalho MT, & Lamond AI (1992) Transcription-dependent colocalization of the U1, U2, U4/U6 and U5 snRNPs in coiled bodies. *Journal of Cell Biology* 117:1-14.

45. Zeng C, Kim E, Warren SL, & Berget SM (1997) Dynamic relocation of transcription and splicing factors dependent upon transcriptional activity. *The EMBO Journal* 16:1401-1412.
46. Hu Y, Kireev I, Plutz M, Ashourian N, & Belmont AS (2009) Large-scale chromatin structure of inducible genes: transcription on a condensed, linear template. *J Cell Biol* 185:87-100.
47. Hu Y, Plutz M, & Belmont AS (2010) Hsp70 gene association with nuclear speckles is Hsp70 promoter specific. *J Cell Biol* 191:711-719.
48. Jolly C, Vourc'h C, Robert-Nicoud M, & Morimoto RI (1999) Intron-independent association of splicing factors with active genes. *J Cell Biol* 145:1133-1143.
49. Everett RD & Murray J (2005) ND10 components relocate to sites associated with herpes simplex virus type 1 nucleoprotein complexes during virus infection. *J Virol* 79(8):5078-5089.
50. Everett RD*, et al.* (1998) The disruption of ND10 during herpes simplex virus infection correlates with the Vmw110- and proteasome-dependent loss of several PML isoforms. *J Virol* 72(8):6581-6591.
51. Pranchevicius MC*, et al.* (2008) Myosin Va phosphorylated on Ser1650 is found in nuclear speckles and redistributes to nucleoli upon inhibition of transcription. *Cell Motil Cytoskeleton* 65:441-456.
52. Gieni RS & Hendzel MJ (2009) Actin dynamics and functions in the interphase nucleus: moving toward an understanding of nuclear polymeric actin. *Biochem Cell Biol* 87:283-306.
53. Houseley J & Tollervey D (2009) The many pathways of RNA degradation. *Cell* 136:763-776.
54. Hofmann WA*, et al.* (2004) Actin is part of pre-initiation complexes and is necessary for transcription by RNA polymerase II. *Nat Cell Biol* 6:1094-1101.
55. Hofmann WA, Johnson T, Klapczynski M, Fan JL, & de Lanerolle P (2006) From transcription to transport: emerging roles for nuclear myosin I. *Biochem Cell Biol* 84:418-426.
56. Da Costa XJ, Kramer MF, Zhu J, Brockman MA, & Knipe DM (2000) Construction, phenotypic analysis, and immunogenicity of a UL5/UL29 double deletion mutant of herpes simplex virus 2. *J Virol* 74:7963-7971.
57. Cliffe AR, Garber DA, & Knipe DM (2009) Transcription of the herpes simplex virus latency-associated transcript promotes the formation of facultative heterochromatin on lytic promoters. *J Virol* 83(16):8182-8190.
58. Godowski PJ & Knipe DM (1986) Transcriptional control of herpesvirus gene expression: gene functions required for positive and negative regulation. *Proc Natl Acad Sci U S A* 83:256-260.
59. Fontaine-Rodriguez EC & Knipe DM (2008) Herpes simplex virus ICP27 increases translation of a subset of viral late mRNAs. *J Virol* 82(7):3538-3545.

Figure Legends

Figure 1. RCs move and coalesce inside the infected cell nucleus.

A cell infected with ICP8-GFP virus was imaged in 4D, starting at 4 hpi. The time series is displayed as a maximum intensity projection. Arrowheads point to four RCs that coalesce during the course of the movie. Lower row shows the same time series with nuclear outlines. Scale bar=5μm.

Figure 2. **Directed motion requires nuclear actin, myosin I, and transcription.**

Movement of RCs was analyzed in 4D and classified into directed motion, simple diffusion or obstructed diffusion using a hierarchical approach based on both the 3D relative shape anisotropy (κ^2) and anomalous diffusion coefficient (α).

(A) Sample 3D trajectories and their ellipsoid of gyration are shown along with their κ^2 values which are defined as a function of the squared length of the semi-axes of the ellipsoid. Trajectories I and II represent non-directed motion and III represents directed motion.

(B) Corresponding MSD curves (blue) and fitted curves (red) are shown. Based on their α values, trajectories I and II (from panel A) are further classified as obstructed diffusion and simple diffusion, respectively.

(C) Distribution of types of RC motion in control cells, cells treated with BDM or lat A at 3 hpi, cells treated with either α-amanitin or cycloheximide at 4 hpi, and cells transfected with plasmids encoding dominant negative nuclear myosin I (NMI-E407V) or actin (Actin-G13R), or with a plasmid encoding wild-type actin

(Actin-NLS). Trajectories were classified as directed motion (red), simple diffusion (green) or obstructed diffusion (blue). The distribution of motion types is displayed as a percentage of the total number of RCs in each experiment.

Figure 3. RCs are associated with nuclear speckles.

(A) Cells were processed for indirect immunofluorescence at various times post infection to detect nuclear speckles and RCs using SC35 (red) and ICP8 (green) antibodies, respectively. High-magnification images of insets are shown in the lower three rows.

(B) Cells were treated with either control medium, lat A or BDM at 1hpi or with α-amanitin at 4 hpi and processed for indirect immunofluorescence to detect SC35 (red) and ICP8 (green) at 4.5hpi. Scale bar = 5μm.

Figure 4. RCs coalesce at nuclear speckles.

(A, B) Cells were transfected with a plasmid encoding mCh-SC35 for 24 hrs and then infected with ICP8-GFP virus and imaged at 4 hpi. Four major types of RC movement (arrow heads), relative to speckles (asterisks), are shown in rows 1-3. Rows 1a and 1b are high magnification time-series images of the cell shown in A and show RCs (green) that move alone, either towards a speckle (red; 1a) or another RC (1b). Rows 2 and 3 are high magnification time-series images of the cell in B and represent RCs that move on speckles or with speckles, respectively. Time stamps in A and B show hr:min:sec post infection. Time stamps in 1-3 show min:sec (at 4 hpi). Scale bars = 5μm. See also Movie S2.

(C) mCh-SC35 transfected cells were treated with control medium, lat A or BDM at 3 hpi, or with α-amanitin at 4 hpi, and imaged at 4 hpi. Numbers of RC coalescence events and types 1-3 movement were determined manually. The data is presented as mean percentage ± SEM per nucleus (~7 nuclei and ~44 RCs were analyzed per treatment). Asterisks mark values that are statistically different from control medium-treated cells ($p<0.05$). See also Movies S2-5.

Figure 5. Effect of directed RC movement on viral gene expression and DNA replication.

Infected cells were incubated with lat A, BDM, or control medium at 3 hpi and harvested at 3, 7 and 12 hpi for RNA, protein and DNA analysis. *ICP27, ICP8* and *gC* were chosen for analysis to represent the IE, E, and L gene classes, respectively.

(A) RNA samples were analyzed by RT-qPCR. Viral RNA levels were normalized to 18S rRNA levels and further normalized to control 12 hpi values. Mean values ± SEM are shown.

(B) Western blot analysis of ICP27, ICP8 and gC protein levels.

(C) Quantification of bands in Western blots. Shorter exposure blots whose values were within the linear range of the film were used for quantitations. Values were normalized to GAPDH and then to control 12 hpi values for each drug treatment. Mean values ± SEM are shown.

(D) Viral DNA levels were analyzed by qPCR using primers specific for the *ICP27* gene. Levels were normalized to cellular sonic hedgehog gene (*SHH*) levels and then to control 12 hpi values. Mean values ± SEM are shown.

Figure 6. Role of directed RC movement in nuclear export of viral RNA.

Cells were treated with control medium, lat A or BDM at 3 hpi and harvested at 12 hpi for nuclear (N) and cytoplasmic (C) RNA.

(A) Ethidium bromide-stained RNA is shown in the top panel to confirm fractionation by the presence of 28S and 18S rRNA in the cytoplasm. Northern blot analysis for *gC* RNA is shown in the bottom panel. RNA samples used in the Northern blot were analyzed by RT-qPCR and the values are displayed on the bottom of each lane as a percentage of total RNA (N+C).

(B) Fractionated RNA was analyzed by RT-qPCR for the presence of *ICP27*, *ICP8*, *gC* and *ICP5* RNA. Amounts were normalized to 18S rRNA. Lat A and BDM values were further normalized to control values and mean ± SEM are shown (n=3 experiments).

Figure 7. Actively transcribing RCs move toward and coalesce at speckles to form RNA export/processing structures.

(A, B) Progeny DNA (black) in a stationary RC undergoes actin- (blue) and RNA pol II (white)-mediated transcription (yellow) of true late genes such as *gC*. (C,D) Myosin (pink) is recruited to the transcribing RC and triggers movement of the RC away from the associated speckle. (E) The mobile RC moves toward

another RC-associated speckle and moves on the surface of the speckle to merge with the other RC. (F) Coalescence of RCs on the speckle surface leads to a reorganization of RCs, allowing for efficient incorporation of RNA processing factors and the processing of true late transcripts in the speckle, ultimately creating an RNA export/processing hub.

Figure 1

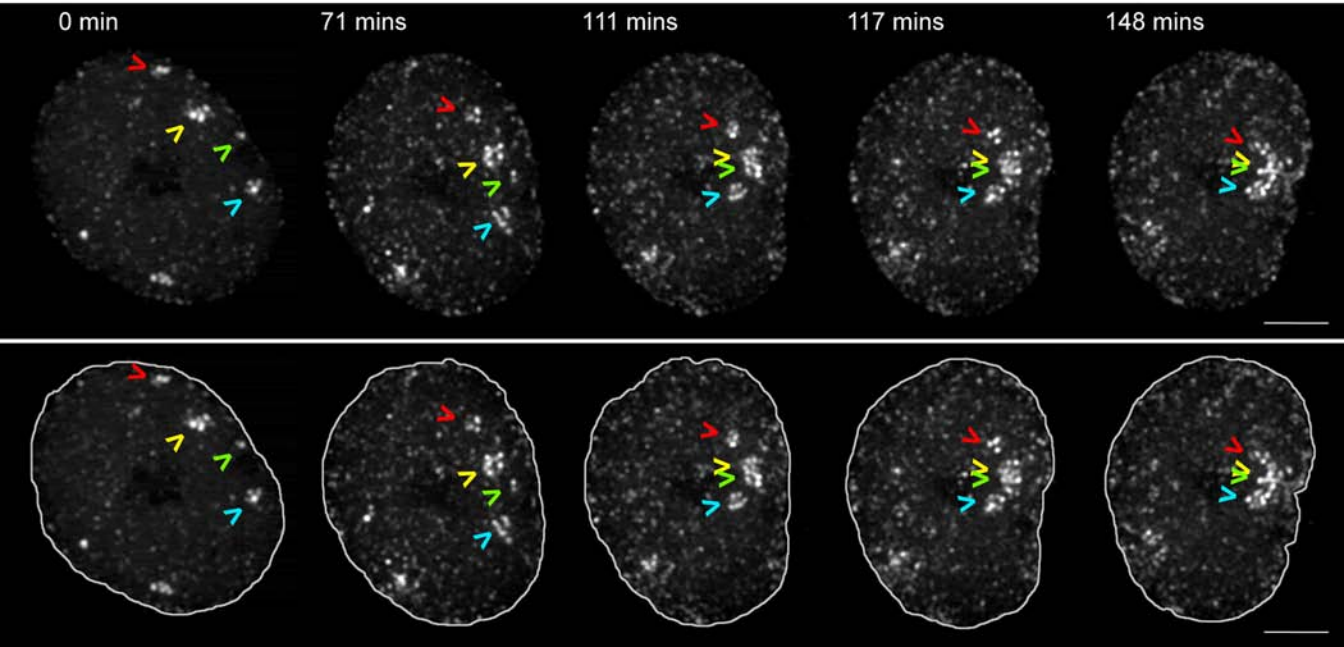

Figure 2

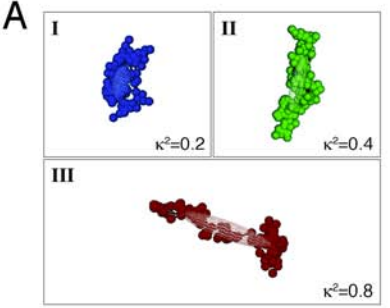
A
I
II
III
κ²=0.2
κ²=0.4
κ²=0.8

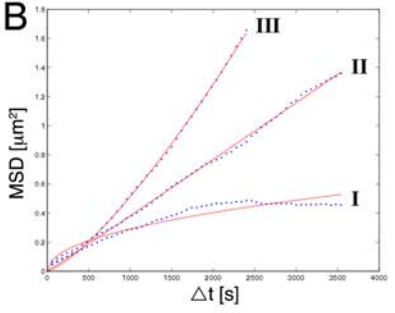
B
III
II
I
MSD [μm²]
△t [s]

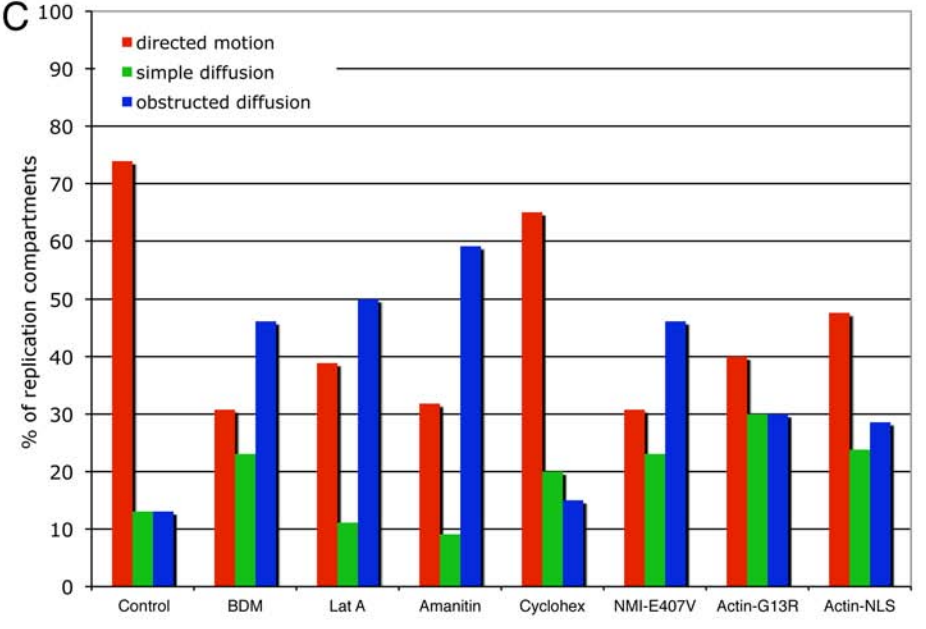
C
directed motion
simple diffusion
obstructed diffusion
% of replication compartments
100
90
80
70
60
50
40
30
20
10
0
Control
BDM
Lat A
Amanitin
Cyclohex
NMI-E407V
Actin-G13R
Actin-NLS

Figure 3

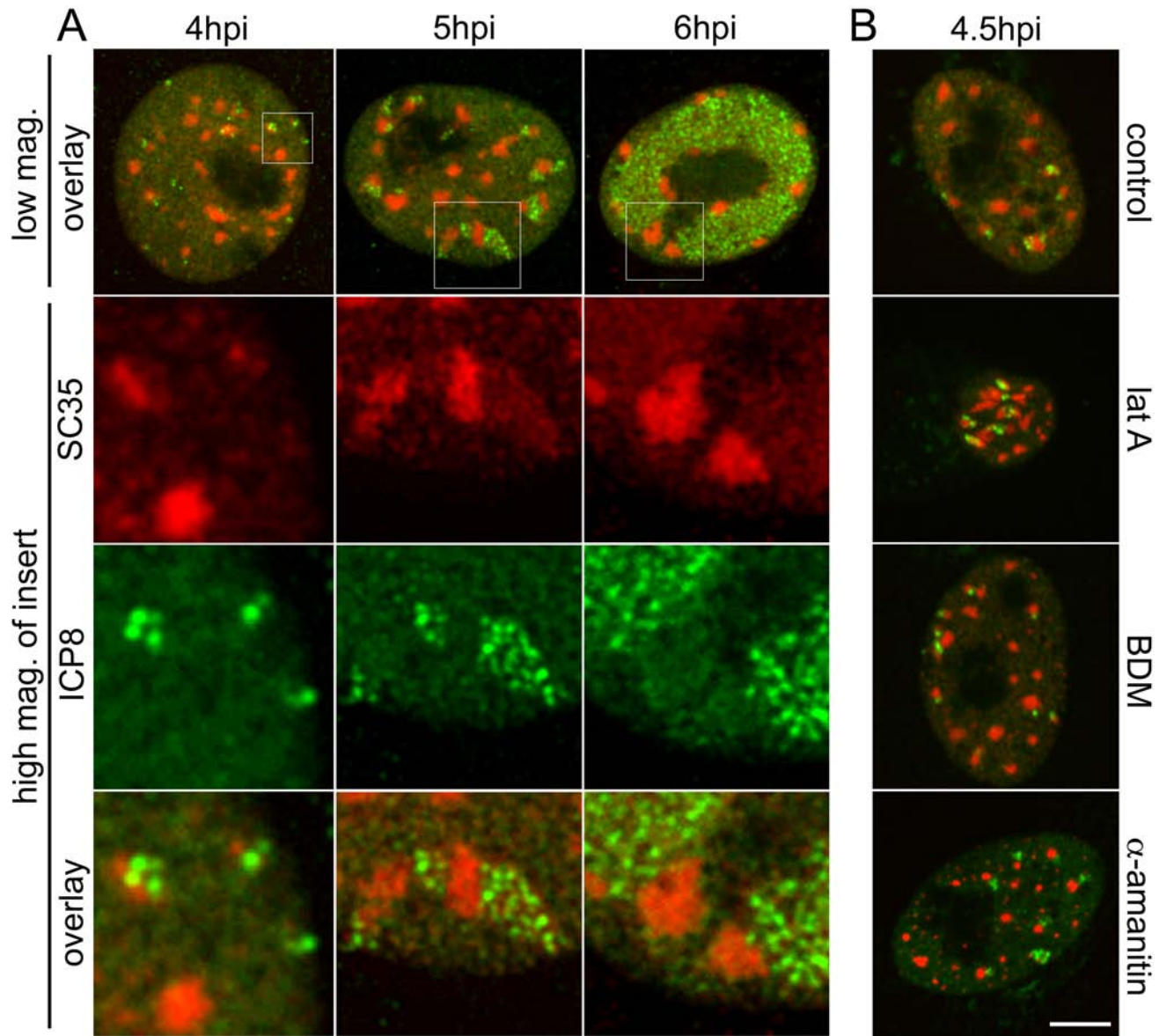
A
4hpi
5hpi
6hpi
B
4.5hpi
low mag.
overlay
high mag. of insert
SC35
ICP8
overlay
control
lat A
BDM
α-amanitin

Figure 4

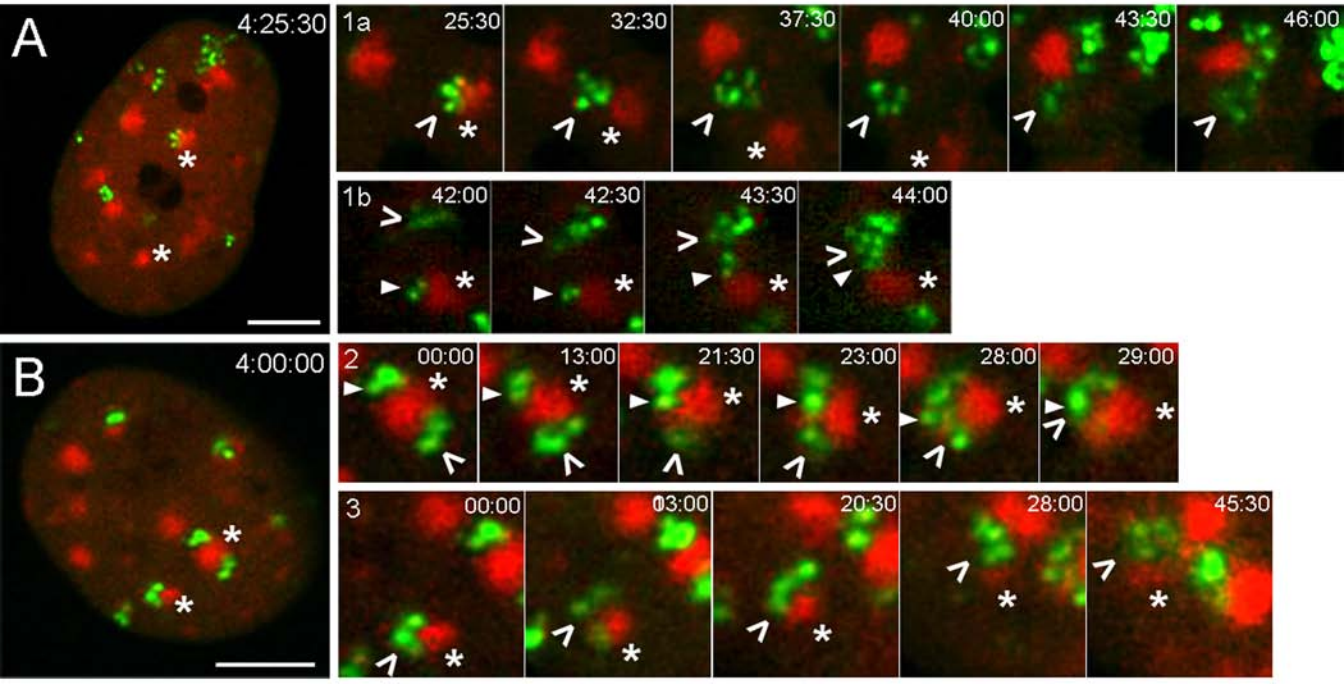
A
4:25:30
1a
25:30
32:30
37:30
40:00
43:30
46:00
1b
42:00
42:30
43:30
44:00
B
4:00:00
2
00:00
13:00
21:30
23:00
28:00
29:00
3
00:00
03:00
20:30
28:00
45:30

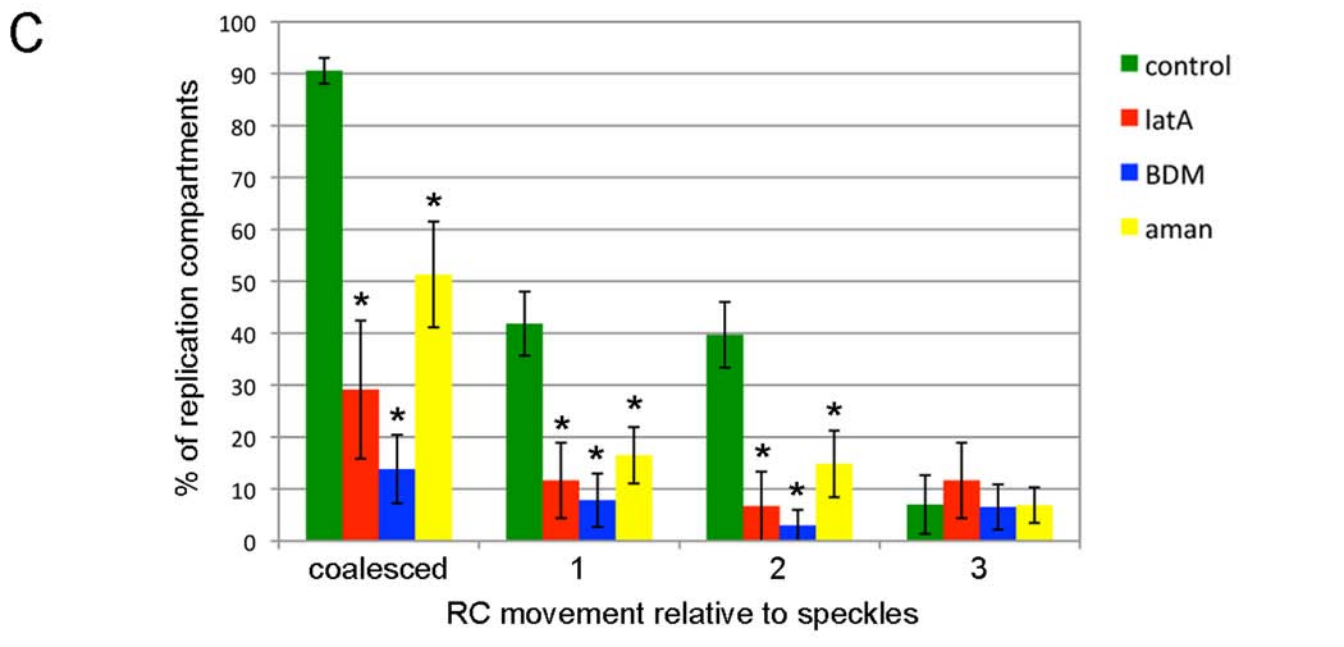
C
% of replication compartments
100
90
80
70
60
50
40
30
20
10
0
coalesced
1
2
3
RC movement relative to speckles
control
latA
BDM
aman

Figure 5

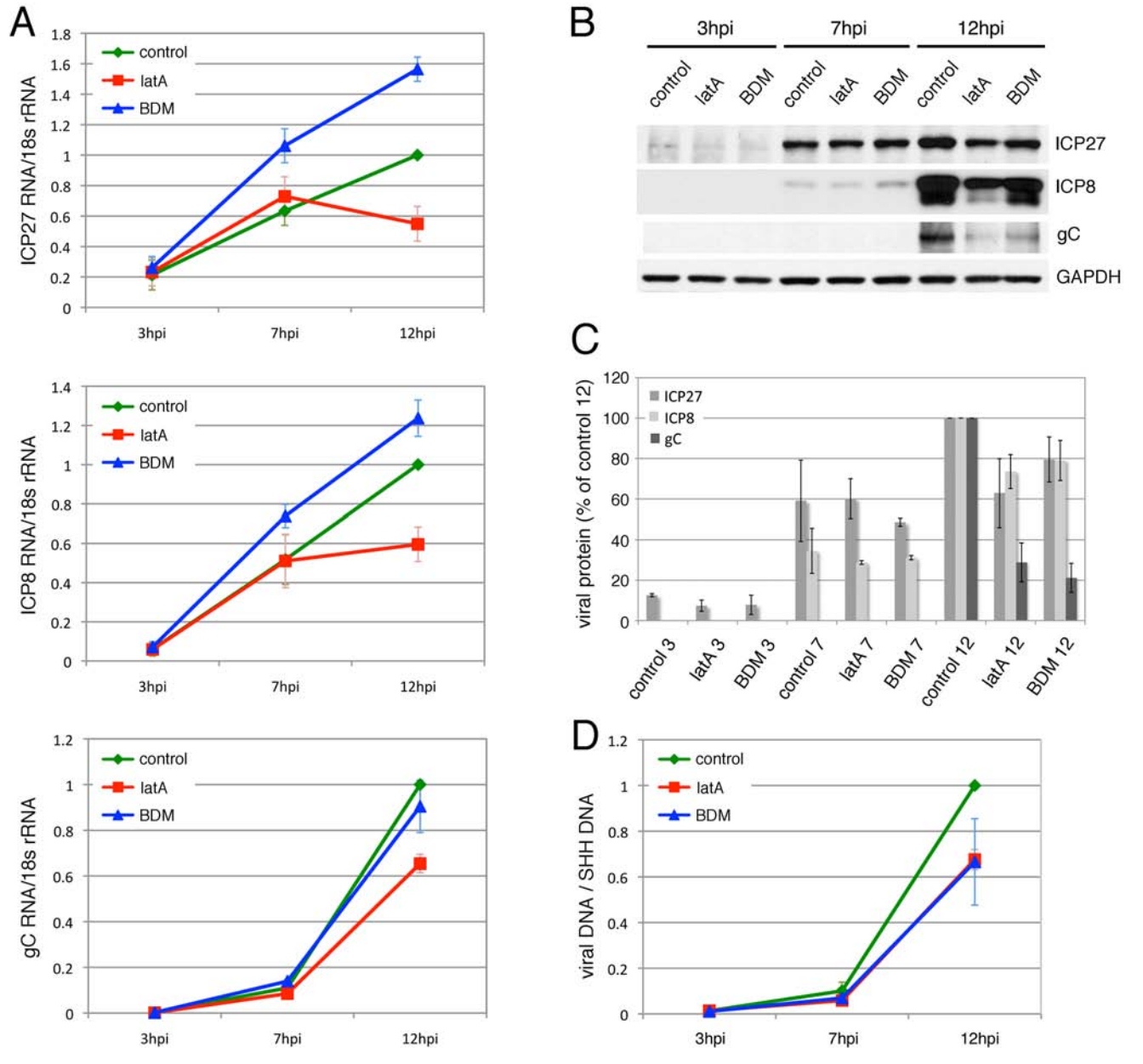
A
ICP27 RNA/18s rRNA
control
latA
BDM
3hpi
7hpi
12hpi
ICP8 RNA/18s rRNA
gC RNA/18s rRNA
B
3hpi
7hpi
12hpi
control
latA
BDM
ICP27
ICP8
gC
GAPDH
C
viral protein (% of control 12)
ICP27
ICP8
gC
control 3
latA 3
BDM 3
control 7
latA 7
BDM 7
control 12
latA 12
BDM 12
D
viral DNA / SHH DNA

Figure 6

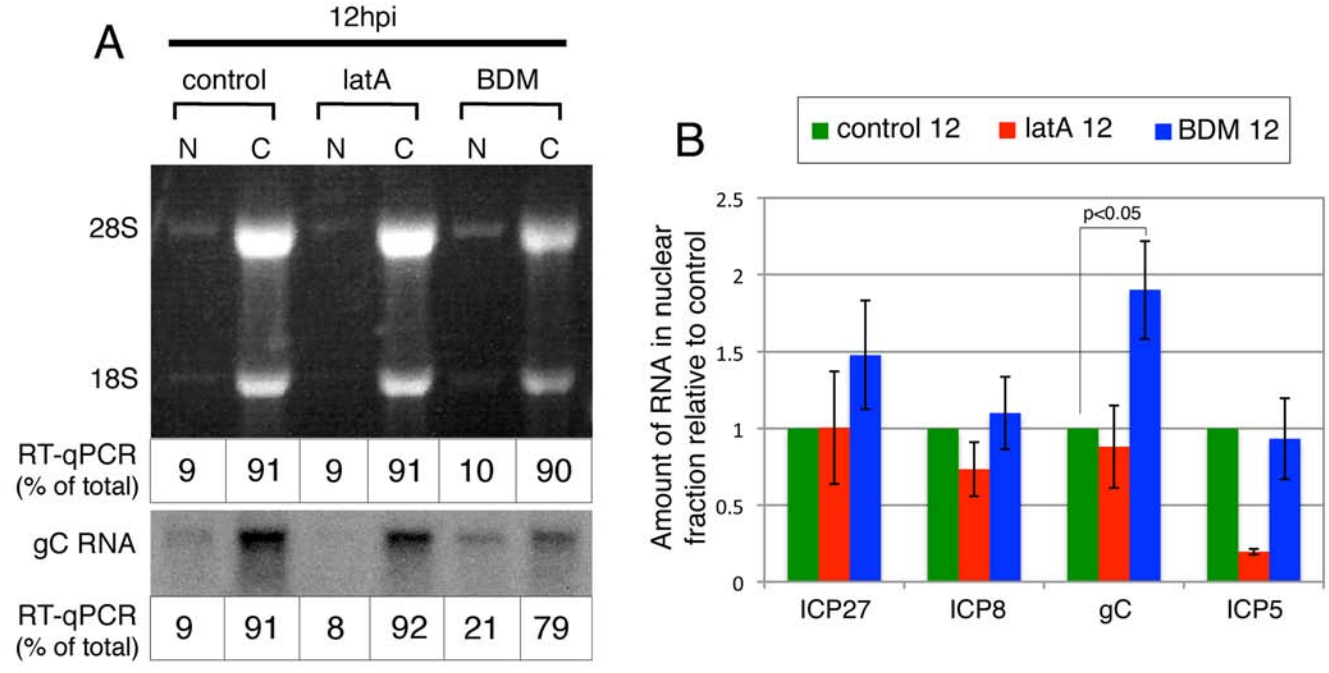
A
12hpi
control
latA
BDM
N
C
N
C
N
C
28S
18S
RT-qPCR (% of total)
9
91
9
91
10
90
gC RNA
RT-qPCR (% of total)
9
91
8
92
21
79
B
control 12
latA 12
BDM 12
Amount of RNA in nuclear fraction relative to control
2.5
2
1.5
1
0.5
0
p<0.05
ICP27
ICP8
gC
ICP5

Figure 7

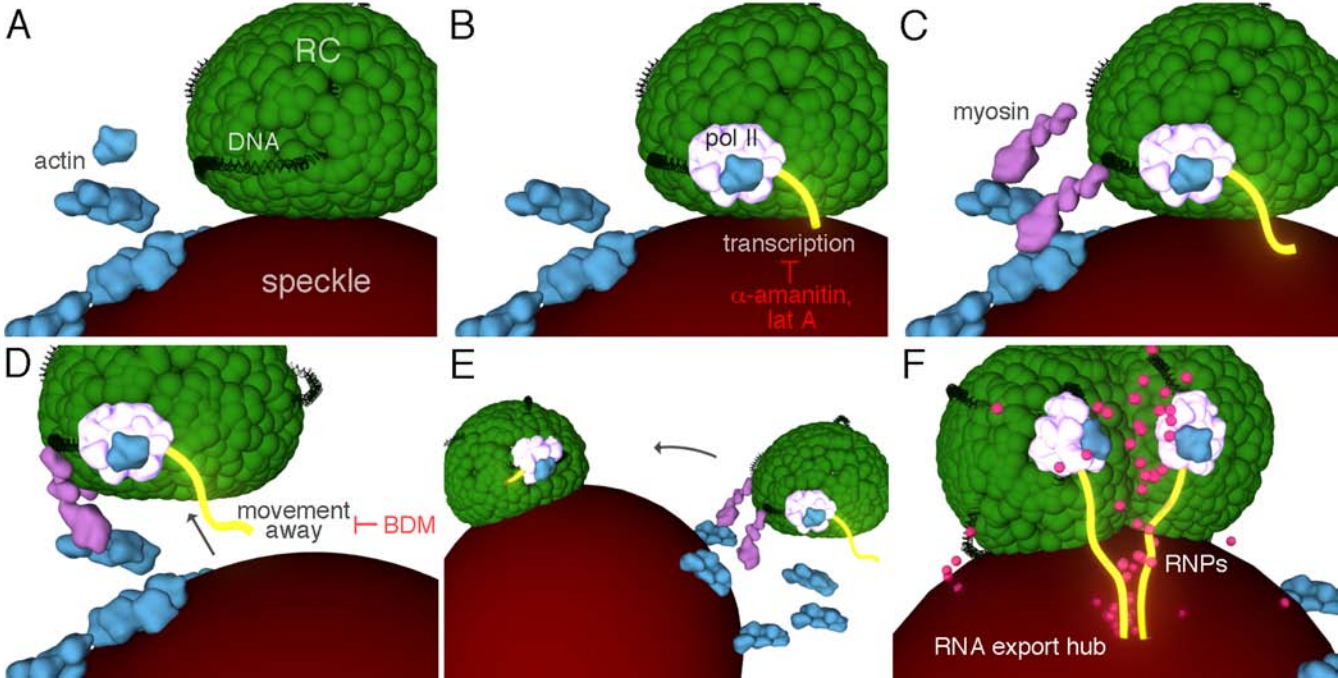
A
RC
DNA
actin
speckle
B
pol II
transcription
α-amanitin,
lat A
C
myosin
D
movement
away
BDM
E
F
RNPs
RNA export hub

Table S1. Statistical Analysis of the Distribution of κ^2 Values in Different Experimental Groups.

Group I	Group II	p-value*
control	BDM	0.011
control	latrunculin A	0.006
control	NMI-E407V	0.001
control	Actin-G13R	0.013
control	Actin-NLS	0.038
Actin-G13R	Actin-NLS	0.395
NMI-E407V	Actin-NLS	0.208
control	α-amanitin	0.002
control	cycloheximide	0.355
α-amanitin	cycloheximide	0.024
BDM	latrunculin A	0.74
BDM	α-amanitin	0.221
latrunculin A	α-amanitin	0.674
NMI-E407V	Actin-G13R	0.897
BDM	NMI-E47V	0.892
latrunculin A	Actin-G13R	0.781

*p-value based on comparison of κ^2 values of Group I versus Group II as determined by Kolmogorov-Smirnov test. An average of four nuclei and 22 RCs were analyzed per treatment.

Supporting Information

Supplemental Data

Movie S1. A maximum intensity projection movie of a cell that has been infected with the ICP8-GFP virus for four hours. A z-stack image was captured every 30 sec for three hours.

Movie S2. Shown is a cell transfected with mCherry-SC35 for 24 hrs and infected with the ICP8-GFP virus. Movie was captured at 4 hpi every 30 seconds, for 79.5 mins. SC35 is shown in red and ICP8 in green.

Movie S3. Shown is a cell transfected with mCherry-SC35 for 24 hrs and infected with the ICP8-GFP virus. At 3 hpi, the cell was treated with lat A and imaged at 4 hpi with 30 sec time intervals, for 58 mins. SC35 is shown in red and ICP8 in green.

Movie S4. Shown is a cell transfected with mCherry-SC35 for 24 hrs and infected with the ICP8-GFP virus. At 3 hpi, the cell was treated with BDM and imaged at 4 hpi with 30 sec time intervals, for 90 mins. SC35 is shown in red and ICP8 in green.

Movie S5. Shown is a cell transfected with mCherry-SC35 for 24 hrs and infected with the ICP8-GFP virus. At 4 hpi, the cell was treated with α-amanitin and imaged immediately thereafter, with 30 sec time intervals, for 90 mins. SC35 is shown in red and ICP8 in green.

Definitions of terms used in RC tracking and trajectory analysis

trajectory: A track connecting the 3D positions of an object (here: individual RCs) at each time point within a time-series. A trajectory represents the path of the movement of an object.

mean square displacement (MSD): A measure of the average distance of the movement of an object. The shape of the MSD curve over time indicates the motion type.

simple diffusion: Typical diffusion process, where the MSD increases linearly with time.

directed motion: Super-diffusive process, where the MSD increases faster than linearly with time.

anomalous diffusion: Sub-diffusive process, where the MSD increases slower than linearly with time.

anomalous diffusion coefficient (α): Parameter that describes the non-linearity of the MSD curve over time.

obstructed and confined diffusion: Subclasses of anomalous diffusion (sub-diffusive process), where the MSD increases slower than linearly with time. Obstructed and confined diffusion can be further classified based on the anomalous diffusion coefficient: $0.1 \leq \alpha < 0.9$ for obstructed diffusion and $\alpha < 0.1$ for confined diffusion.

3D relative shape anisotropy (κ^2): Parameter used to characterize the three dimensional shape of a trajectory. Directed motion corresponds to trajectories with a more elongated or anisotropic shape (κ^2 values are close to 1). Simple

diffusion (or random motion) corresponds to trajectories with a more spherical or isotropic shape (κ^2 values close to 0).

ellipsoid of gyration: An ellipsoid that characterizes the asymmetry of a trajectory. The semi-axes of the ellipsoid correspond to the principal axes of the trajectory (collection of 3D positions). The elongation or anisotropy of the ellipsoid is determined by the lengths of its semi-axes.

Extended Experimental Procedures

Plasmids used for transfections

Plasmids encoding NMI-E407V, actin-G13R and actin-NLS are described in (1) and (2). The mCherry-lamin A plasmid (mCh-LA) used for tracking nuclear position is described in (3). The mCh-SC35 plasmid was constructed by excising the SC35 ORF out of a pCMV-YPF-N1-SC35 plasmid (4) and sub-cloning into an mCherry-N1 vector.

4D tracking

We developed fully automated approaches for image registration as well as for tracking multiple replication compartments. Briefly, to remove the translational and rotational motion of the nucleus (visualized by the mCherry-lamin A localization), we developed a rigid registration approach. With this approach, the following steps were carried out: for each time step of an image sequence, we detected the image region corresponding to the nucleus using a 3D Gaussian filter and an intensity threshold. The values for the standard

deviations σ_{xy} and σ_z of the Gaussian filter were chosen based on the size of the nucleus (typically we used values of σ_{xy} = 10 and σ_z = 2 voxels). The position of the nucleus was determined by computing the center-of-mass of the corresponding voxel positions, while the orientation was obtained by diagonalizing the covariance matrix of the voxel positions. Each time step *t* of the image sequence was aligned to time step 0 by computing a rigid transformation based on the position and orientation of the nucleus at both time steps. Subsequently, we applied an intensity-based rigid registration scheme (5). Because of photobleaching, the intensities of the first time step differed strongly from those of the latter time steps. Without proper compensation for this variation, finding a correct transformation between the first and the latter time steps based on their intensities may be challenging. To cope with this, we applied the registration approach to consecutive time steps of the image sequence, thereby obtaining a rigid transformation between time steps *t* and *t* + 1. By recursively concatenating the sequential transformations, we computed the required transformation between time steps 0 and *t*. We applied this registration approach to the images in the mCherry channel. The resulting transformations were also applied to the corresponding images in the GFP channel. We used the registered 3D image sequences as input for the tracking approach. For tracking multiple replication compartments, we developed a probabilistic approach (6). At each time step of an image sequence, our approach performs four steps: 1) detection and localization of compartments, 2) prediction of the position of the tracked compartments, 3) matching of the predicted positions with the detected

compartments, and 4) position estimation. To detect and localize the compartments, image regions corresponding to the objects of interest were enhanced using a 3D Laplacian-of-Gaussian filter (7, 8). The values for the standard deviations σ_{xy} and σ_z of the filter were chosen based on the size of the compartments (usually we used values of σ_{xy} = 5 and σ_z = 3 voxels). After filtering, an intensity threshold was computed from the mean intensity of the image plus a factor *c* times the standard deviation of the image intensities; the threshold was applied to the image to detect regions corresponding to compartments. To identify these regions, we employed a connected-components labeling algorithm (6-connectivity), which groups spatially adjacent detected voxels by analyzing the local neighborhood (consisting of six voxels) around each considered voxel. The position of each compartment was determined by computing the center-of-mass. To calculate a prediction for the position of each tracked compartment we used a spatial-temporal filter (in this case, a Kalman filter with a Brownian motion model). To find the correspondence between a predicted position and a detected compartment, we employed a global nearest-neighbor approach (9). Based on the predicted and detected position estimates, the final position estimate of a tracked compartment was computed using the spatial-temporal filter.

RC motion analysis

To determine the motion type of individual compartments, we developed a hierarchical approach based on both the anomalous diffusion coefficient α (10)

as well as the 3D relative anisotropy κ^2 (11, 12). To obtain an estimate for the anomalous diffusion coefficient (α) of a trajectory, we computed the mean-square displacement (MSD) as a function of the time interval Δt. We fitted the anomalous diffusion model $MSD = 6D\Delta t^{\alpha}$ (10) to the calculated MSD values, thereby obtaining an estimate for the diffusion coefficient D as well as for the anomalous diffusion coefficient α. To improve the accuracy of the estimates (10), we restricted the MSD calculations to time intervals Δt smaller than $N/3$, where N is the total number of available positions in the trajectory. To characterize the shape of the trajectory via its 3D relative anisotropy κ^2, we first calculated the squared radius of gyration s^2, the asphericity b, and the acylindricity c, using the eigenvalues of the covariance matrix of the trajectory's positions. Based on these shape measures, we calculated the relative shape anisotropy $\kappa^2 = (b^2 + 0.75c^2) / s^4$. Note that $\kappa^2 \in [0, 1]$, where values close to 0 correspond to trajectories with an isotropic shape (i.e., trajectories exhibiting random motion) while values tending towards 1 correspond to trajectories with an anisotropic shape (i.e., trajectories displaying directed motion). We thus used κ^2 as our criterion to detect directed motion using a threshold value of $\kappa^2 = 0.5$. This threshold value was determined using simulated trajectories where the true motion type of the trajectories was known. Our hierarchical approach for determining the motion type of the compartments therefore first employed κ^2 to distinguish trajectories exhibiting directed motion from those displaying random motion. We then used the scheme proposed in Bacher et al. (13) to classify the latter into confined diffusion ($\alpha < 0.1$), obstructed diffusion ($0.1 \leq \alpha < 0.9$), or

simple diffusion ($\alpha \geq 0.9$). An average of four nuclei per treatment were analyzed for MSD and anisotropy analyses (~22 RCs per treatment). Two-sample Kolmogorov-Smirnov test (14) was used to determine the statistical significance of differences between experimental groups in cumulative distribution of κ^2 values.

Antibodies used for indirect immunofluorescence and Western Blot experiments

For the indirect immnunofluorescence studies, mouse anti-SC35 (clone SC-35; Sigma-Aldrich; S4045; 1:1000 dilution) and rabbit anti-ICP8 (3-83; 15; 1:500 dilution) antibodies were used. Goat-anti-mouse-Alexa 594 (Invitrogen) and goat-anti-rabbit-Alexa 488 (Invitrogen) were used at a 1:500 dilution for secondary detection.

Antibodies used in Western blot experiments were mouse a-ICP27 (EastCoast Bio; H1A027; 1:2500 dilution), rabbit a-ICP8 (3-83; 15; 1:10000 dilution), mouse a-gC (Virusys; H1A022; 1:2500 dilution), and mouse a-GAPDH (Applied Biological Materials; G041; 1:5000 dilution). HRP-conjugated goat antibodies were used at 1:10000 dilution (Santa Cruz Biotechnology).

Sequences of primers used in RNA-to-Ct 1-step qPCR and standard qPCR reactions

ICP27 (mRNA): 5'- GATTCGGGCCCGGTCGTTGCTAC -3',
5'- CCGTCGGGGCTGGGGTGTC -3'
ICP27 (gene): 5'- CCGCCGGCCTGGATGTGACG -3',
5'- CGTGGTGGCCGGGGTGGTGCTC -3' (16)

ICP8 (mRNA): 5'- CCCAGCACCCAGGCCCCAAACC -3'
5'- AGCGCCTCCCCCGTCGTCTCGT -3',
gC (mRNA): 5'- CCCCCGCGGACCTTCACCT-3',
5'- GGCCGCGGCAGCACCAG -3'
ICP5 (mRNA): 5'- CTTAGCACGATCGAGGT -3';
5'- GTTCATGTAGGCCAGCT -3'
18s rRNA (mRNA): 5'- CATGAACGAGGAATTCCCAGTAA -3',
5'- GATCCGAGGGCCTCACTAAAC -3' (17)
Sonic hedgehog (gene): 5'- CTGATCGATCGTGGGGGTTATGTG -3',
5'- TGCGGGCGTCAGGGTGGAT -3'

Supplemental References

1. Chuang CH*, et al.* (2006) Long-range directional movement of an interphase chromosome site. *Curr Biol* 16:825-831.
2. Posern G, Sotiropoulos A, & Treisman R (2002) Mutant actins demonstrate a role for unpolymerized actin in control of transcription by serum response factor. *Mol Biol Cell* 13:4167-4178.
3. Taimen P*, et al.* (2009) A progeria mutation reveals functions for lamin A in nuclear assembly, architecture, and chromosome organization. *Proc Natl Acad Sci U S A* 106:20788-20793.
4. Prasanth KV, Sacco-Bubulya PA, Prasanth SG, & Spector DL (2003) Sequential entry of components of the gene expression machinery into daughter nuclei. *Mol Biol Cell* 14:1043-1057.
5. Yang S*, et al.* (2008) Nonrigid registration of 3-d multichannel microscopy images of cell nuclei. *IEEE Trans Image Process* 17:493-499.
6. Godinez WJ*, et al.* (2009) Deterministic and probabilistic approaches for tracking virus particles in time-lapse fluorescence microscopy image sequences. *Med Image Anal* 13:325-342.
7. Marr D & Hildreth E (1980) Theory of edge detection. *Proc R Soc Lond B Biol Sci* 207:187-217.
8. Sage D, Neumann FR, Hediger F, Gasser SM, & Unser M (2005) Automatic tracking of individual fluorescence particles: application to the study of chromosome dynamics. *IEEE Trans Image Process* 14:1372-1383.
9. Sbalzarini IF & Koumoutsakos P (2005) Feature point tracking and trajectory analysis for video imaging in cell biology. *J Struct Biol* 151:182-195.
10. Saxton MJ & Jacobson K (1997) Single-particle tracking: applications to membrane dynamics. *Annu Rev Biophys Biomol Struct* 26:373-399.
11. Theodorou DN & Suter UW (1985) Shape of unpreturbed linear polymers: Polypropylene. *Macromolecules* 18:1206-1214.
12. Saxton MJ (1993) Lateral diffusion in an archipelago. *Biophys. J* 64:1766-1780.

13. Bacher CP, Reichenzeller M, Athale C, Herrmann H, & Eils R (2004) 4-D single particle tracking of synthetic and proteinaceous microspheres reveals preferential movement of nuclear particles along chromatin - poor tracks. *BMC Cell Biol* 5:45.
14. Conover WJ (1971) One-sample "Komogorov" test/ Two-sample "Smirnov" test. *Practical nonparametric startitics*, ed Wiley B (John Wiley & Sons, New York, NY), pp 295-301, 309-314.
15. Knipe DM, Senechek D, Rice SA, & Smith JL (1987) Stages in the nuclear association of the herpes simplex virus transcriptional activator protein ICP4. *J Virol* 61:276-284.
16. Cliffe AR, Garber DA, & Knipe DM (2009) Transcription of the herpes simplex virus latency-associated transcript promotes the formation of facultative heterochromatin on lytic promoters. *J Virol* 83:8182-8190.
17. Wright PJ, Crameri G, & Eaton BT (2005) RNA synthesis during infection by Hendra virus: an examination by quantitative real-time PCR of RNA accumulation, the effect of ribavirin and the attenuation of transcription. *Arch Virol* 150:521-532.